CONF-8708191--1

CONF-8708191--1

DE88 002945

Three-Dimensional Contact/Impact Methodology

by

R. F. Kulak

DISCLAIMER

1 INTRODUCTION

The simulation of three-dimensional interface mechanics between reactor components and structures during static contact or dynamic impact is necessary to realistically evaluate their structural integrity to off-normal loads. In our studies of postulated core energy release events, we have found that significant structure-structure interactions occur in some reactor vessel head closure designs and that fluid-structure interactions occur within the reactor vessel. Other examples in which three-dimensional interface mechanics play an important role are: (1) impact response of shipping casks containing spent fuel, (2) whipping pipe impact on reinforced concrete panels or pipe-to-pipe impact after a pipe break, (3) aircraft crash on secondary containment structures, (4) missiles generated by turbine failures or tornados, and (5) drops of heavy components due to lifting accidents. The above is a partial list of reactor safety problems that require adequate treatment of interface mechanics. Contact/impact problems are also present in the automotive, aircraft, rail, and weapons industries.

Contact/impact methodology is an area that has received increased attention in the past decade. A large number of the methods reported, however, are limited to infinitesimal motion, node-to-node contact, and/or two-dimensional geometries. However, many of our problems are three-dimensional and involve large motions. Essentially, at an interface between two bodies compatibility and conservation of momentum should be satisfied. An attempt to satisfy these two conditions, in varying degrees, is made by the methods that have been proposed in the literature. For example, with the Lagrange Multiplier approach (e.g. Hughes et al. (1976)) compatibility is exactly enforced, but conservation of momentum is accounted for with discrete impact and release conditions. Also, the contact stresses are treated as unknowns and thus increase the size of the problem. For problems in which 30 to 50 percent of the nodes are on the contacting surface, the size increase is significant. Regularization methods have been used by Nichols and Hirt (1978) and also by Belytschko and Mullen (1981) to smooth the discontinuous transition between pre- and post-impact velocities. Momentum is conserved by regularization, and the compatibility condition is only approximated. Another approach is the penalty method (e.g. Key et al. (1978), Hallquist (1978), Marti (1983), and Kulak (1985a)) which essentially inserts interface springs

between the impacting surfaces. This approach conserves momentum without the need for impact and release conditions; however, the compatibility condition is approximately satisfied. A perturbed Lagrangian formulation was developed by Simo et al. (1985) in which the contact constraint is enforced in an "average" sense on each contact segment.

Here we present a method that may be used to model three-dimensional contact/impact mechanics in which large sliding can occur. A family of finite elements based upon the penalty method are developed. The contact elements consists of a base, which is affixed to one body and an apex node which is affixed to another. Explicit forms for nodal contact forces are developed for a tetrahedral element with a triangular base, a triangular element with a line base, and a line element with a point base. An adaptive connectivity algorithm is developed to handle problems with finite sliding in which the contact nodes travel across element boundaries. An adjacency table, which contains all the contact elements and their contiguous neighbors, is used to monitor the location of each apex node as it travels from one element base to another during impact and/or sliding between the two bodies. This methodology has been incorporated into the NEPTUNE code (Kulak (1980)).

2 CONTACT MECHANICS

Consider two bodies B^1 and B^2 (Figure 1) that are in contact along a common surface S_c, which can vary in size during the interaction. Let S_c^α be the part of the surface of body B^α (α=1,2) that belons to S_c. Define a triad of unit vectors ($\underset{\sim}{n}$, $\underset{\sim}{s}$, $\underset{\sim}{m}$) along the contact surface, S_c. Let $\underset{\sim}{n}$ be normal to the surface, let $\underset{\sim}{s}$ lie in the direction of relative sliding, and let $\underset{\sim}{m}$ be orthogonal to $\underset{\sim}{n}$ and $\underset{\sim}{s}$. For each body we define the vectors as follows:

$$(1) \qquad \underset{\sim}{n} = \underset{\sim}{n}^1 = -\underset{\sim}{n}^2 \quad \text{and} \quad \underset{\sim}{s} = \underset{\sim}{s}^1 = \underset{\sim}{s}^2 .$$

The normal component of the Cauchy traction vector, $\underset{\sim}{\sigma}^\alpha$, on S_c^α is given by

$$\sigma_n^\alpha = \underset{\sim}{\sigma}^\alpha \cdot \underset{\sim}{n}^\alpha ,$$

$$(2)$$

$$\underset{\sim}{\sigma}_n^\alpha = \sigma_n^\alpha \, \underset{\sim}{n}^\alpha$$

During contact the normal tractions satisfy the relation

$$(3) \qquad \underset{\sim}{\sigma}_n^1 = -\underset{\sim}{\sigma}_n^2 ,$$

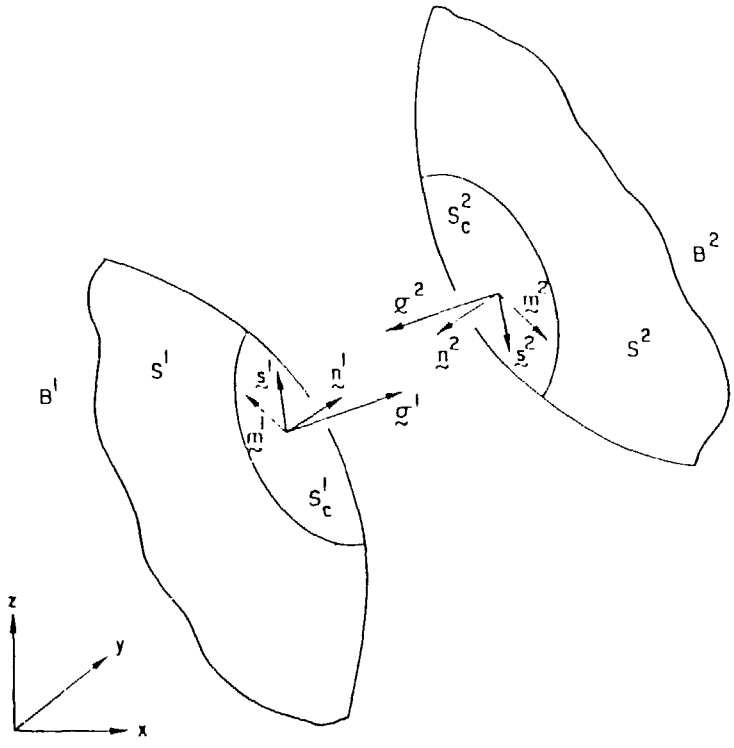

Figure 1. Contacting Bodies.

and when the surfaces are not in contact, the tractions are zero, that is

$$\underset{\sim}{\sigma}_n^1 = \underset{\sim}{\sigma}_n^2 = 0 \ . \tag{4}$$

Only negative normal tractions are permitted along the interface because adhesion is not permitted; thus

$$\sigma_n \leq 0 \quad \text{on} \quad S_c \tag{5}$$

when the two bodies are in contact, their normal velocities are equal along S_c, thus

$$\underset{\sim}{v}_n^1 = \underset{\sim}{v}_n^2 \ . \tag{6}$$

Because penetration of one body into the other is not permitted, the following unilateral contact conditions applies;

$$g_n > 0 \quad \text{on} \quad S_c \tag{7}$$

where g_n is the gap normal to the interface.
The rate-of-change in normal traction is computed from

$$\dot{\sigma}_n = \begin{cases} E\,\dot{h} & \text{if} \quad h < h_c \\ 0 & \text{if} \quad h > h_c \end{cases} \tag{8}$$

where E is a resistance modulus, h is the current height of the contact element, which is the distance between S_c^1 and S_c^2, and h_c is the height at which contact occurs. Thus, if the height of the element is greater than the contact height, the traction is zero; otherwise, a normal traction is generated. Since the traction, σ_n, is corotational, it is updated as follows

$$\sigma_n(t + \Delta t) = \sigma_n(t) + \dot{\sigma}\,\Delta t \ , \tag{9}$$

where t is the time, and Δt is the time step.
By employing the principal of virtual power we can obtain an equivalent nodal forces from the normal traction distributions over the contact surface; thus

$$\int_{S_c} \sigma_n\,\dot{g}_n\,dS_c = f^n_{iI}\,v_{iI} \tag{10}$$

in which f^n_{iI} is the nodal force due to the normal tractions at node I in the ith global coordinate direction, v_{iI} are the velocity components, and g_n is the rate-of-change in gap. If we assume that $\dot{g}_n$ is given by the linear form

$$\dot{g}_n = B^n_{iI}\,v_{iI} \ , \tag{11}$$

and then invoke the arbitrariness of the nodal velocities, we have

$$f^n_{iI} = \int_{S_c} \sigma_n\,B^n_{iI}\,dS_c \ . \tag{12}$$

In the following section we will obtain explicit forms of the nodal forces for a pyramidal element with a quadrilateral base, a triangular element, and a line element. Note, in the remainder of our work, we assume that the normal tractions are uniform over the base of each contact element.

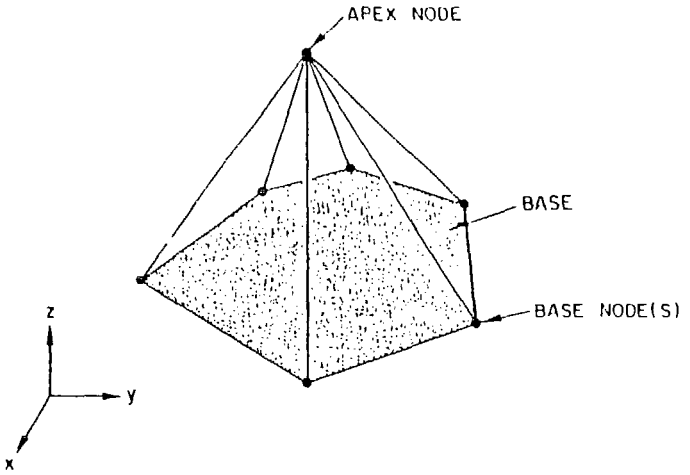

Figure 2. Generic Interface Element with a Base and Apex

3 CONTACT ELEMENTS

The elements that are used at the interface have certain common attributes, which we will now describe. Each element consists of an apex node and a base (Figure 2). The base may consist of one or more nodes. The base is formed from nodes belonging to one body, and the apex is a node from the other body. Note, this is a nonsummetric or master-slave treatment. A symmetric interaction is achieved by defining element bases and apexes on both contacting surfaces; this would require twice as many contact elements. At this point we point out that the same nodes always form the base of each element, but because of the adaptive nature of this method different nodes can be the apex. The element height, h, is the normal distance from the base to the apex node. The rate-of-change in element height, $\dot{h}$, is given by

$$\dot{h} = B_{iI}\, v_{iI} \,. \tag{13}$$

Kennedy and Belytschko (1983) used this form for two-dimensional geometries, and Kulak (1985a, 1985b) applied it in three-dimensions. A comparison of equations 11 and 13 show that the rate-of-change in gap is equal to the rate-of-change in element height: $\dot{g}_n = \dot{h}$.

3.1 Tetrahedral element

In this subsection we present the derivation of a tetrahedral contact element that has a triangular base.

We position nodes 1-2-3 on the base and let node 4 form the apex (Figure 3). We will assume that the height is given by

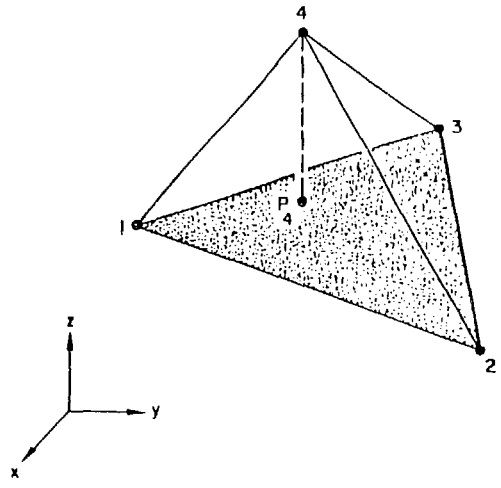

Figure 3. Tetrahedral Interface Element with a Triangular Base

$$h = \frac{3\,V}{A} \tag{14}$$

where V is the volume of a tetrahedron and A is the area of the base.

Our task now is to compute the B_{iI} coefficients of equation 13 for the element. The rate-of-change in element height is given by the relation

$$\dot{h} = \frac{3}{A}\dot{V} - \frac{3V}{A}\dot{A} = B_{iI}\,v_{iI}\,, \tag{15}$$

The volume for a pyramid is obtained from the volume formula which is given by

$$6V = \begin{vmatrix} 1 & x_1 & y_1 & z_1 \\ 1 & x_2 & y_2 & z_2 \\ 1 & x_3 & y_3 & z_3 \\ 1 & x_4 & y_4 & z_4 \end{vmatrix}\,, \tag{16}$$

where x_I, y_I, and z_I are the global coordinates for node I. The area of the triangular base is given by

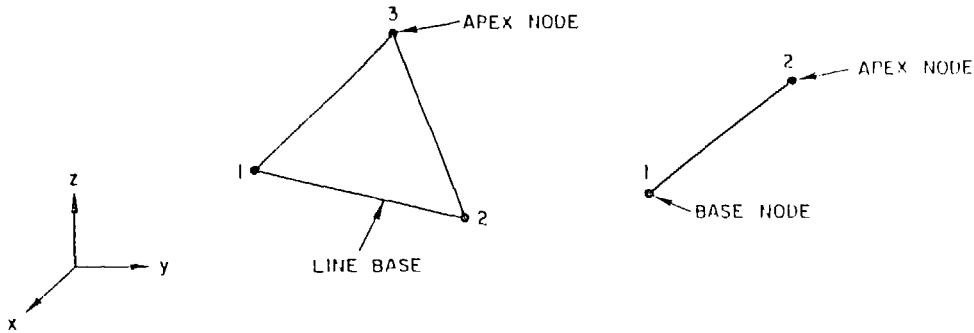

Figure 4. (a) Triangular Interface Element and
(b) Line Interface Element.

$$(17) \qquad A = \left[\frac{1}{4}\left(y_{21}\, z_{31} - y_{31}\, z_{21}\right)^2 + \frac{1}{4}\left(z_{21}\, x_{31} - z_{31}\, x_{21}\right)^2 + \frac{1}{4}\left(y_{31}\, x_{21} - y_{21}\, x_{31}\right)^2\right]^{0.5} ,$$

which can be rewritten as

$$(18) \qquad A = \left[A_x^2 + A_y^2 + A_z^2\right]^{0.5} ,$$

where A_x, A_y, A_z are projected areas defined in equation 17. The B_{II} coefficients are obtained by substituting the temporal derivatives of the volume and area into equation 15. The internal force expression for the tetrahedron is obtained by evaluating equation 12, which gives the following simple form

$$
(19)\quad
\begin{Bmatrix}
f^{int}_{x1} \\ f^{int}_{y1} \\ f^{int}_{z1} \\ f^{int}_{x2} \\ f^{int}_{y2} \\ f^{int}_{z2} \\ f^{int}_{x3} \\ f^{int}_{y3} \\ f^{int}_{z3} \\ f^{int}_{x4} \\ f^{int}_{y4} \\ f^{int}_{z4}
\end{Bmatrix}
= f
\begin{Bmatrix}
c_1(y_2z_{43} + y_3z_{24} + y_4z_{32}) + c_2(\Lambda_y z_{32} + \Lambda_z y_{23}) \\
c_1(z_2x_{43} + z_3x_{24} + z_4x_{32}) + c_2(\Lambda_x z_{23} + \Lambda_z x_{32}) \\
c_1(x_2y_{43} + x_3y_{24} + x_4y_{32}) + c_2(\Lambda_x y_{32} - \Lambda_y x_{23}) \\
c_1(y_3z_{41} + y_4z_{13} + y_1z_{34}) + c_2(\Lambda_y z_{13} + \Lambda_z y_{31}) \\
c_1(z_3x_{41} + z_4x_{13} + z_1x_{34}) + c_2(\Lambda_x z_{31} + \Lambda_z x_{13}) \\
c_1(x_3y_{41} + x_4y_{13} + x_1y_{34}) + c_2(\Lambda_x y_{13} + \Lambda_y x_{31}) \\
c_1(y_4z_{21} - y_1z_{24} - y_2z_{41}) + c_2(\Lambda_y z_{21} + \Lambda_z y_{12}) \\
c_1(z_4x_{21} - z_1x_{24} - z_2x_{41}) + c_2(\Lambda_x z_{12} + \Lambda_z x_{21}) \\
c_1(x_4y_{21} - x_1y_{24} - x_2y_{41}) + c_2(\Lambda_x y_{21} + \Lambda_y x_{12}) \\
c_1(y_1z_{23} + y_3z_{12} + y_2z_{31}) \\
c_1(z_1x_{23} + z_3x_{12} + z_2x_{31}) \\
c_1(x_1y_{23} + x_3y_{12} + x_2y_{31}) \ ,
\end{Bmatrix}
$$

and the constants are given by

$$
(20)\qquad c_1 = 0.5/\Lambda_{123} \ , \quad c_2 = -1.5V/(\Lambda_{123})^3 \ , \quad f = \sigma_n \Lambda_{123} \ .
$$

Λ_{123} is the area of face 1-2-3.

3.2 Triangular and line elements

In order to treat problems in which finite sliding occurs over curved surfaces, we found it necessary to use two additional contact elements: a triangular element (Figure 4a) and a line element (Figure 4b). These elements were previously derived by Kulak (1985a) using the approach outline in the previous section. Here we will only give the forms for the nodal contact forces.

The explicit form for the global nodal contact forces of our triangular contact element is given by

$$(21)\qquad \begin{Bmatrix} f_{x1} \\ f_{y1} \\ f_{z1} \\ f_{x2} \\ f_{y2} \\ f_{z2} \\ f_{x3} \\ f_{y3} \\ f_{z3} \end{Bmatrix} = \frac{f}{2AL_{21}} \begin{Bmatrix} A_y z_{32} + A_z y_{23} + c_3 x_{12} \\ A_x z_{23} + A_z x_{32} + c_3 y_{12} \\ A_x y_{32} + A_y x_{23} + c_3 z_{12} \\ A_y z_{13} + A_z y_{31} + c_3 x_{21} \\ A_x z_{31} + A_z x_{13} + c_3 y_{21} \\ A_x y_{13} + A_y x_{31} + c_3 z_{21} \\ A_y z_{21} + A_z y_{12} \\ A_x z_{12} + A_z x_{21} \\ A_x y_{21} + A_y x_{12} \end{Bmatrix} ,$$

where the constant c_3 is given by

$$(22)\qquad c_3 = -2(A/L_{21})^2 ,$$

and Ax, Ay, Az are projected areas.

The global nodal contact forces for our line element are given by

$$(23)\qquad f_{iI} = f\ B_{iI} = \frac{f}{h} \begin{Bmatrix} X_{21} \\ Y_{21} \\ Z_{21} \end{Bmatrix} ,$$

where h is the distance between the two nodes.

4 ADAPTIVE CONNECTIVITY

For the purpose of treating problems with finite sliding, it is necessary to allow the apex node the freedom to be connected to different bases at different times during the simulation. There is no

unique method to determine this adaptive connectivity. The method we propose is simple, efficient, and capable of handling the problem that we had to deal with to-date. Other more encompassing algorithms could be developed, if needed, but would probably be more complicated and computationally expensive.

During the discretization of a problem, potential contact elements are defined. Each of these elements consists of a base and an apex node. The specific node(s) that form the base of the element are defined by the user and remain fixed throughout the numerical simulation. In contrast, the apex node of the element can change during the simulation. In fact, it is possible that during some point in the simulation an element will not have an apex node and would be considered a null element, that is an element which does not participate in the calculations. It is also possible for an element to have more than one node associated with its base. Thus, we see that a specific apex node can be associated with different contact elements at different times during the simulation.

In order to reduce the computational time required when a search is performed to identify the element that an apex node is associated with, we utilized a contact element adjacency table. For each pyramidal contact element, the table contains the element numbers of all the contiguous pyramidal contact elements. Thus, when a specific apex node fails to project itself onto the base that it was previously identified with, the adjacency table contains the information needed to reconnect the apex node to another base.

Now we address the task of dynamically adapting the connectivity of the contact elements. At this point, it is worth emphasizing the fact that an element's connectivity only changes during a small percentage of the computational steps. At the end of each computational cycle, the connectivity of each tetrahedral contact element is checked to see if its apex node (1) continues to project onto its current base, (2) projects onto an adjacent base, or (3) does not project onto any base. The determination of node projection is performed in the following manner. When an apex node projects inside its currently defined base (Figure 5) then the natural coordinates of the projection, L_1, L_2, and L_3 should satisfy the relation

$$0 < L_I < 1 \qquad (I = 1,3) \; . \tag{24}$$

The values of the natural coordinates are obtained from the following procedure. First, the largest component of the nodal force of the apex node, f_{m4}, is identified from

$$f_{m4} = \max \left(f_{x4}, f_{y4}, f_{z4}\right) \; , \tag{25}$$

where the subscript m indicates the coordinate direction with the largest force component. Then the value of the shape functions for the base nodes are calculated as

$$N_I = - \frac{f_{mI}}{f_{m4}} \; . \qquad (I = 1,3) \tag{26}$$

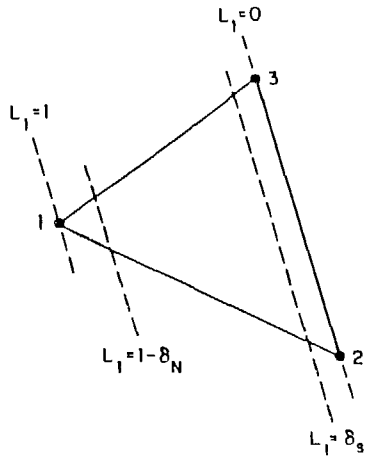

Figure 5. Triangular Base of Tetrahedral Element

Note, the shape functions, N_I, for the triangular base are identical to the natural coordinates, L_I. If the computed values for L_I satisfy equation 24 then the apex projects onto its current base. In addition, if the natural coordinates satisfy the relation

$$\delta < L_I < 1 - \delta \quad (I = 1,3) \tag{27}$$

then the apex projects onto the interior region of the base and the previously calculated nodal forces (i.e. equation 19) are valid.

If the natural coordinates satisfy only equation 24, then the apex projects onto the boarder region of the base, which is near the sides and corners of the base. We have elected to give this situation special treatment, similar to the approach of Marti (1983), to provide a smoother transition between bases. When the following conditions hold,

$$L_I < \delta, \quad L_J < 1 - \delta, \quad L_K < 1 - \delta, \tag{28}$$

then the apex is projecting onto a boarder region next to the side opposite node I. When the following condition is true,

$$L_I > 1 - \delta, \tag{29}$$

the apex node is projecting into the corner at node I.

We use the following procedure to treat the above two cases. When the apex node projects into the side region of the boarder, we generate a so-called phantom triangular contact element along that side. The line base of the triangular element is defined by the two

nodes of the side, and the apex node for the triangular element is the apex node of the pyramidal element. For this situation, we can think of the pyramidal contact element as being replaced by a temporary triangular element, and in this localized region of S_c the contact between the two bodies is a node-to-line contact. Since this element does not exist in the problem's connectivity array, it is thought of as a phantom element. It becomes visible only when the above logic path is transversed.

When the apex node projects into the corner region of the boarder, we activate a phantom line contact element with the corner node as the base node. For this condition the localized contact between the two bodies is a node-to-node contact.

For the case when equation 24 is not satisfied, then the apex does not project onto the current base, and we must determine (1) if the apex does project onto another base, and (2) if it does which base is it. An element adjacency table is used to identify the contact elements adjacent to the sides and corners of the current contact element. Note, we used an element adjacency table in the quasi-Eulerian methodology (Kulak (1984)), which is embedded in NEPTUNE, and have borrowed those data structures for our contact algorithm. To briefly illustrate, if JE is a contact element, S_I (I = 1,3) is a contact element adjacent to side I, and C_I (I = 1,12) is a contact element adjacent to corner I, then the entries in the adjacency table would be as follows: IADJT (1,JE) = S_1, ... IADJT (5,JE) = C_1, ... IADJT (12,JE) = C_{12}. The current values of L_I are used to determine which side or corner that the apex node had possibly passed through. The values for L_I are now recalculated relative to the potential new base, to see if they satisfy equation 24. If equation 24 is satisfied, then the apex node is removed from the connectivity array of the original base and added to the connectivity of the new base. Nodal contact forces are calculated in the next step, as described above, using the new base. All adjacent bases are eventually searched.

When the mesh configuration is such that the bases lie on a convex surface, then it is possible for the apex node to lie in regions that do not belong to any element projections. For example, there is a "trough" shaped region, as shown in Figure 6a, that lies along the common line connecting the triangular bases of adjacent tetrahedral contact elements. In addition, a "pyramid" shaped region (Figure 6b) exists at the vertices of adjacent elements. When the bases lie on a concave surface, the opposite problem occurs; the apex node may project onto more than one base. For this situation, we activate either a phantom triangular contact element or a phantom line element, depending upon the current value of the natural coordinates. The apex node is considered to belong to the current base, and phantom elements are invoked until the apex projects onto a base, either its current base or a new base.

5 NUMERICAL EXAMPLES

The following examples are presented to verify our newly developed numerical formulation for treating the interface mechanics between two bodies and to illustrate its use in modeling reactor structural safety problems in which impact, contact, and/or sliding take place between components.

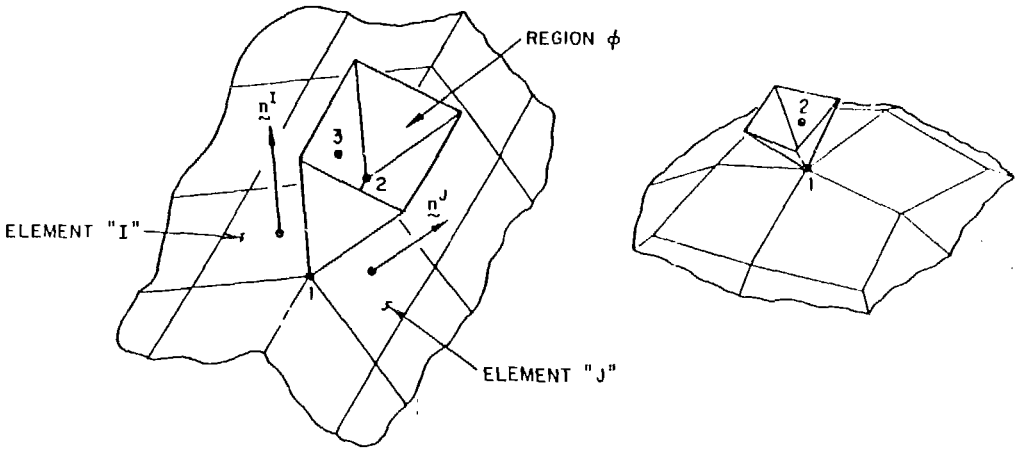

Figure 6. (a) Trough Region Along Common Side of Adjacent Bases and (b) Pyramidal Region at Corner of Adjacent Bases

5.1 Two impacting bars

Our first example is the longitudinal impact of two identical elastic bars. Although this problem is relatively simple, it proved to be very useful in checking out the interface element. The analytical solution which is available is used to benchmark our numerical results. We assume that bar 1 (Figure 7a) had an initial velocity of 0.1 and that bar 2 is initially at rest. The area of each bar is 10.0, length is 100.0, Young's modulus is 100.0 and the density is 0.01. Note that we used dimensionless quantities. Our finite element mesh is shown in Figure 7b, and it consists of 20 axial elements per bar with a tetrahedral gap-contact element between them. The interface force, Figure 8, was in good agreement with the analytical solution.

5.2 JSME shipping cask benchmark calculations

Recently, the Subcommittee on Structural Analysis of Nuclear Shipping Casks of the Japan Society of Mechanical Engineers (JSME) conducted a benchmark study to identify methods that were suitable for modeling the impact response of spent nuclear fuel shipping casks. Some of these results were reported by Yagawa et al. (1984), and we decided to compare them with NEPTUNE calculations to help verify the interface element.

One of the problems in the JSME study was the impact response of an assembly of a thin-wall stainless steel cylindrical shell that contained a lead cylinder. The assembly is dropped from a height of 9.0 m onto a rigid floor. It should be noted that large relative motions (sliding) occurred between the steel shell and the lead cylinder. Therefore, this problem provided a check on the ability of our newly developed interface element to model sliding between two bodies. The material properties of the lead are as follows: density = 1.13×10^{-9} kg-s/mm^4, Young's modulus = 19.5 kg/mm, Poisson's ratio =

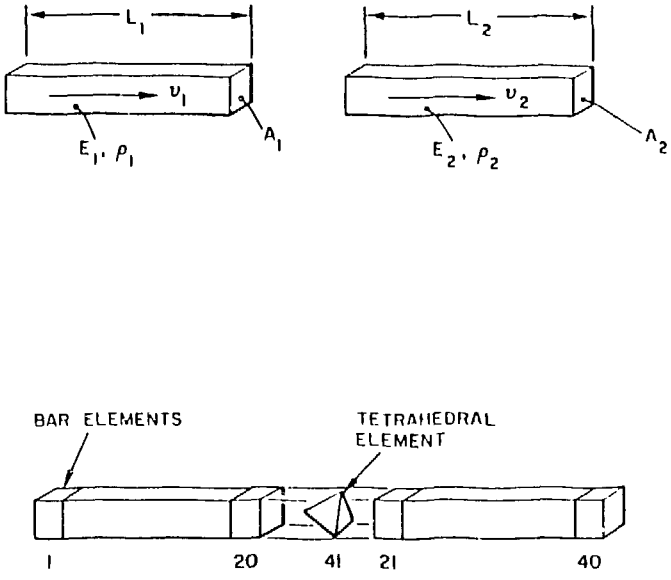

Figure 7. (a) Two Impacting Bars and (b) Finite Element Model of Impacting Bars

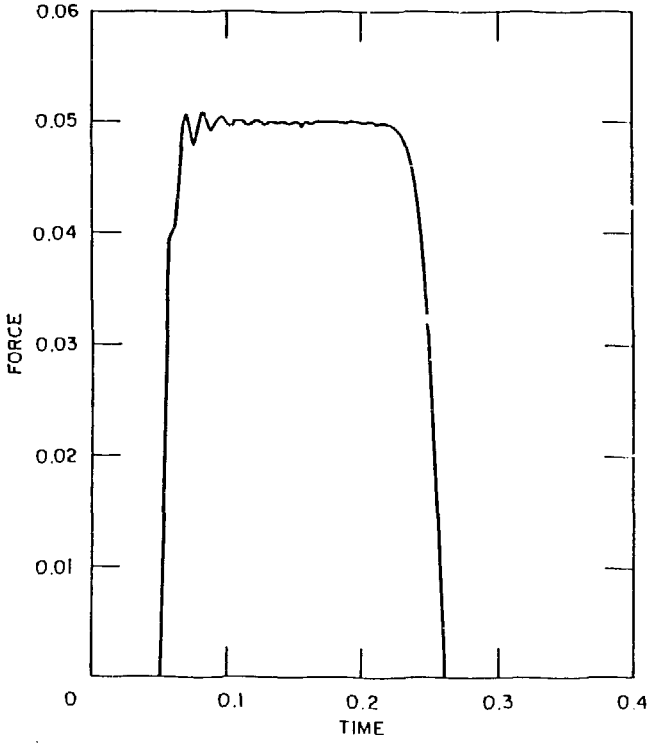

Figure 8. Temporal Evolution of Interface Force

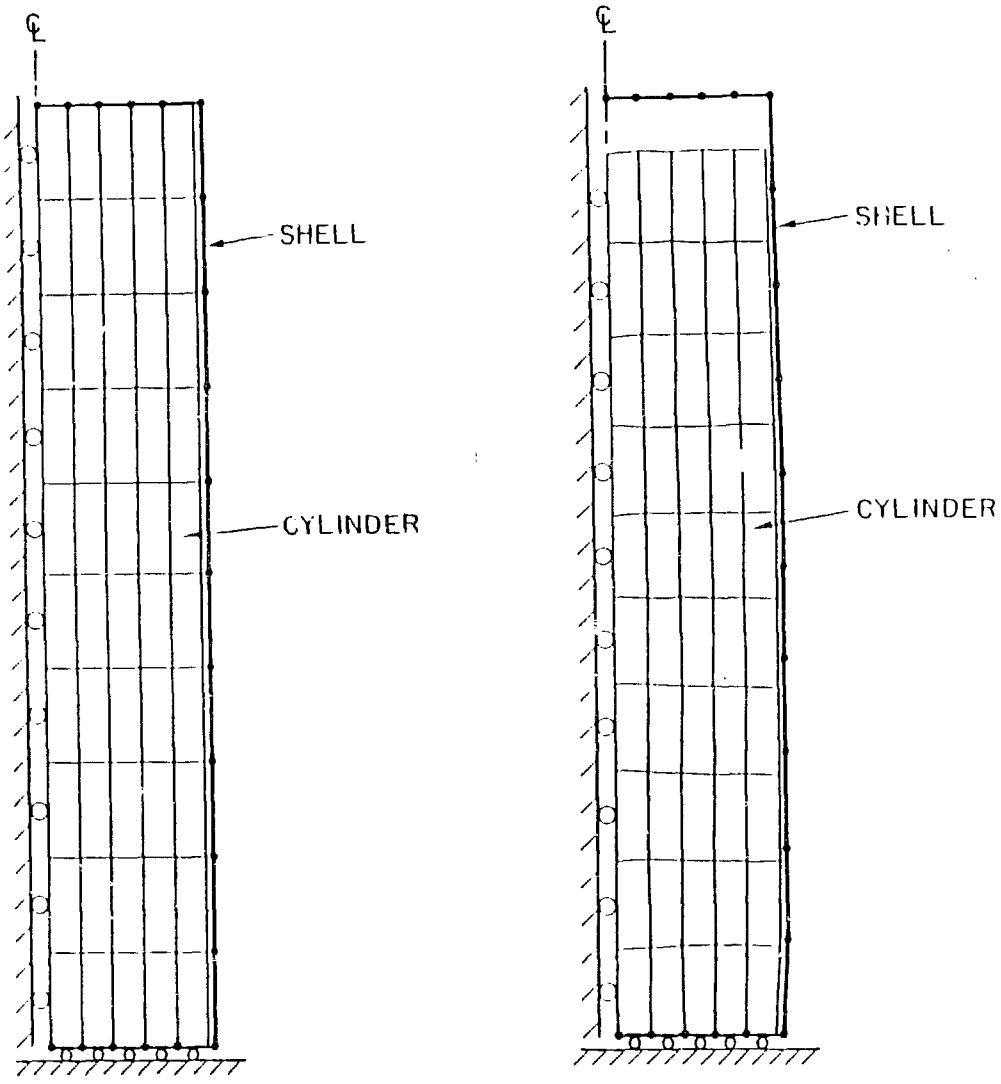

Figure 9. (a) Finite Element Model for Impacting Cladded Cylinder and (b) Deformed Shape at 5 ms After Impact

0.42, yield stress = 3.02 kg/mm, and tangent modulus = 1.85 kg/mm. The material properties for the steel are density = 8.0×10^{-10} kg-s/mm, Young's modulus = 1.96×10^{4} kg/mm, Poisson's ratio = 0.33, yield stress = 31.6 kg/mm, and tangent modulus = 195.0 kg/mm.

Figure 9a is a view of our model. A 15-degree circumferential sector model was developed. The lead cylinder consists of 50 hexahedral continuum elements: 5 elements in the radial direction and 10 elements in the vertical direction. The cylindrical shell was modeled with NEPTUNE's three-node triangular plate element. Interface elements were inserted between the lead cylinder and steel shell in order to allow sliding and possible separation at the interface. The interface was assumed to be frictionless.

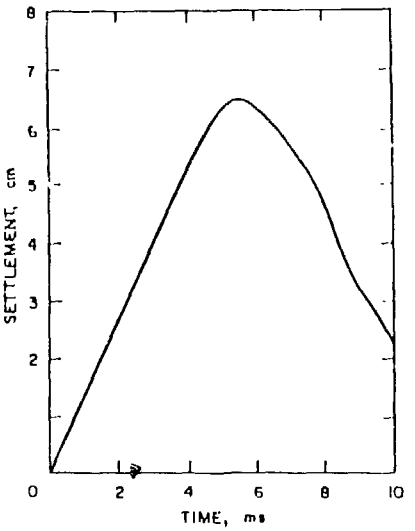

Figure 10. History of Head Settlement

Figure 10 shows the history of the head settlement, which is the displacement of the top of the lead cylinder. The cask impacts against the floor at 0.0 ms. The maximum calculated value for had settlement was 6.5 cm and occurred at 5.5 ms. Yagawa et al. (1984) reported on the results from several organizations which used different computer programs, and Key (1985) reported on his simulations of this problem.

Table 1. Comparison of numerical results from several codes for impact response of a cladding cylinder

Code	Maximum Head Settlement (Cm)	Time (msec)
ABAQUS	7.25	6.25
ANSYS	5.80	4.30
HONDOIII	6.27	5.50
MARC	6.35	5.70
NEPTUNE	6.50	5.50

Table 1 showed the results for maximum head settlement and the time at which it occurred for numerical calculations performed by five different computer programs, including NEPTUNE. The range for maximum head settlement and the time at which it occurred was 5.8 to 7.25 cm and 4.3 to 6.25 m, respectively. Our results compare favorably with the above ranges. Figure 9b shows the deformed configuration of the

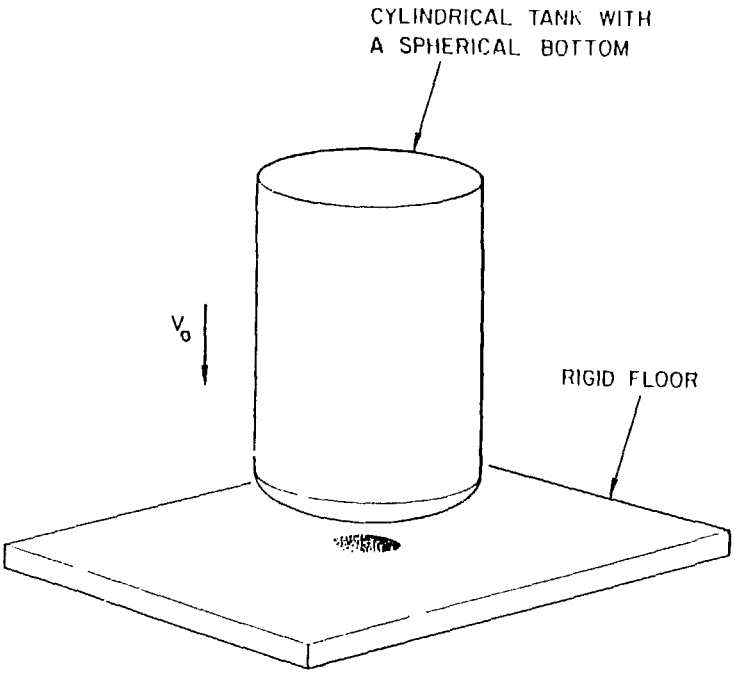

Figure 11. Schematic View of a Cylindrical Tank with a Spherical Bottom Impacting Vertically onto a Rigid Floor

cask at 5 ms; the large sliding between the thin shell and lead is clearly visible.

5.3 Vertical impact of a spherical-bottomed cylindrical tank

The following problem was designed to check the performance of the element in a fairly complex impact situation. Since we constructed this problem, we have no other solution at this time with which to compare our results. Figure 11 is a schematic view of the problem. A 0.25 in. thick cylindrical tank with a spherical bottom was impacted against a rigid floor. For simplicity, gravitational effects were neglected. The cylinder was 12.4 in. long with a diameter of 20 inches. The material properties are as follows: density = 2.45×10^{-4} lb-sec/in^4, Young's modulus = 10.5×10^6 lb/in^2, Poisson's ratio = 0.3, yield stress = 24×10^3 lb/in^2, and tangent modulus = 0.21×10^6 lb/in^2.

The tank was assumed to impact the floor head-on with a velocity of 600 in/sec. By prescribing the impact in this way, only one-quarter of the cylinder needed to be modeled. Also, the head-on impact orientation provided a good check for evaluating the degree to which the symmetry of the response is maintained during the simulation. The finite element model is depicted in Figure 12a, and it consists of 175 quadrilateral plate elements and 47 tetrahedral impact elements. The impact elements are infused between the floor and tank bottom; however, for clarity, the impact elements are not shown. The bases of the tetrahedral elements are located at the surface of the floor, and

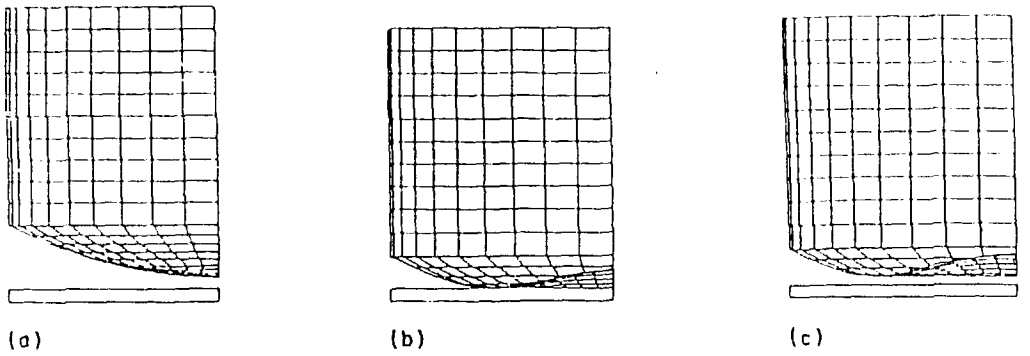

Figure 12. Cylindrical Tank Configuration: (a) Before Impact, (b) During Impact, and (c) After Impact

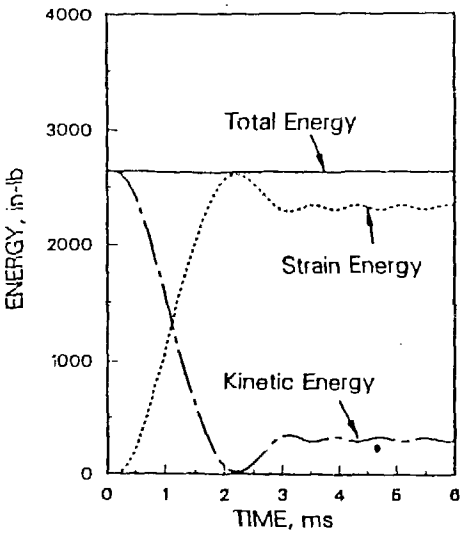

Figure 13. Temporal Evolution of Total Energy, Kinetic Energy, and Strain Energy

the apexes are the nodes of the spherical cap. The rectangle at the bottom of the figure represents the rigid floor. The simulation was started (time = 0.0 s) with the tank bottom being 0.10 in. above the floor in order to see if the contact criteria properly detects contact when the tank reaches the floor. Figure 12b shows the configuration of the impacting cylinder at 2 ms after the beginning of the simulation. Note, the center of the bottom of the tank, which was the first area to make contact with the floor, has rebounded, and the outer part of the tank bottom is now in contact with the floor. In Figure 12c, it is seen that the entire tank has rebounded off the floor. Figure 13 showed the evolution of the total energy, kinetic energy, and strain energy during impact. It was seen that the initial kinetic energy was converted into strain energy as the cylinder comes to rest at 2.16 ms. Most of this strain energy was in the form of plastic strain energy as indicated by the small amount of strain energy that was converted back into kinetic energy during the rebound. The total energy remained nearly constant throughout the calculations, as it should. This checkout problem verified that the previously developed contact and release conditions are satisfactorily treating the mechanics at the impact interface. Although we do not have other results to compare with, we felt that the dynamic response was reasonable, especially in view of the excellent conservation of total energy.

ACKNOWLEDGEMENT

This work was performed under the auspices of the U. S. Department of Energy, Office of Technology Support Program, under contract W-31-109-Eng-38.

REFERENCES

Belytschko, T.B. and Mullen, R. 1981. Two-dimensional fluid-structure impact computations with regularization. Comp. Meth. in Appl. Mech. and Eng. 27:139-154.

Hallquist, J.O. 1978. A numerical treatment of sliding interfaces and impacts. In K.C. Park and D.K. Gartling (eds.), Computational techniques and interface problems, AMD-30, p. 117-133. New York: American Society of Mechanical Engineers.

Hughes, T.J.R., Taylor, R.L., Sackman, J.L., Curnier, A., and Kanoknukulchai, W. 1976. A finite element method for a class of contact-impact problems. Comp. Meth. in Appl. Mech. and Eng. 8:249-276.

Kennedy, J.M. and Belytschko, T.B. 1983. Buckling and post-buckling behavior of the ACS support columns. Nucl. Eng. Des. 75(3):323-342.

Key, S.W., Beisinger, Z.E., and Krieg, R.D. 1978. HONDO-II - a finite element computer program for a large deformation dynamic response of axisymmetric solids.

Key, S.W. 1985. A comparison of recent results from HONDO III with JSME nuclear shipping cask benchmark calculations. Nucl. Eng. Des. 85:15-23.

Kulak, R.F. 1984. A finite element quasi-eulerian method for three-dimensional fluid-structure interactions. Comput. Struct. 18(2) 319-332.

Kulak, R.F. 1985a. Adaptive contact elements for three-dimensional fluid-structure interfaces. In D.C. Ma and F.J. Moody (Eds.), Fluid-structure dynamics, PVP-98-7, p. 159-166. New York:American Society of Mechanical Engineers.

Kulak, R.F. 1985b. Three-dimensional fluid-structure coupling in translent analysis. Comput. Struct. 21(3) 529-542.

Marti, J. 1983. PR3D documentation manual. Tech. Rpt. No. PR-TN-4.32. Principia Mechanica Ltd., London, UK.

Nichols, B.D. and Hirt, C.W. 1978. Numerical simulations of hydrodynamic impact loads on cylinders. EPRI NP-824 Interim Rep. 1978, Electric Power Research Institute, Palo Alto, California.

Simo, J.C., Wriggers, P., and Taylor, R.L. 1985. A perturbed lagrangian formulation for the finite element solution of contact problems. Comp. Meth. in Appl. Mech. and Eng. 50:163-180.

Yagawa, G., Ohtsubo, H., Takeda, H., Toi, Y., Aizawa, T., and Ikushima, T. 1984. A round robin on finite element calculations for impact problems. Nucl. Eng. Des. 78:377-388.